Supporting Information for

Kinetic and Thermodynamic Preferences in Aryl vs. Benzylic C–H Bond Activation with Cationic Pt(II) Complexes

Alan F. Heyduk, Tom G. Driver, Jay A. Labinger*, John E. Bercaw*

Arnold and Mabel Beckman Laboratories of Chemical Synthesis, California Institute of Technology, Pasadena, CA 91125 (U. S. A.)

General considerations. All manipulations were carried out in the inert atmosphere provided by a nitrogen-filled glove box. 2,2,2-Trifluoroethanol-d_3 (TFE-d_3, Cambridge Isotopes) was dried with 3 Å mol sieves, which had been pretreated with acetone-d_6 and activated at 150 °C under dynamic vacuum prior to vacuum distillation. Methylene chloride-d_2, benzene-d_6, *p*-xylene-d_{10}, mesitylene-d_{12} (Cambridge Isotopes), acetonitrile, benzene, *p*-xylene, mesitylene (OMNI Solv), and tris(pentafluorophenyl)borane (Strem) were used as received without further purification. (NN)$PtMe_2$ (NN = 2,3-bis(3,5-dimethylphenylimino)butane) was prepared by the previously reported procedure and gave satisfactory analyses, which were performed at Midwest Microlab, LLC.

NMR spectra were recorded on Varian Mercury 300 (^{1}H, 299.8 MHz; ^{19}F, 282.1 MHz; ^{13}C, 75.4 MHz), Varian Inova 500 (^{1}H, 499.8 MHz) and Varian Inova 600 (^{1}H, 599.8 MHz) spectrometers. ^{1}H NMR data for kinetic runs were collected on the Varian Inova 600 spectrometer at 24(1) °C. NMR spectra were referenced to TMS using the residual ^{1}H and ^{13}C impurities of the given solvent. Chemical shifts are reported using the standard δ notation in parts per million; positive chemical shifts are to a higher frequency from TMS.

"Protonation" of (NN)$PtMe_2$ with $B(C_6F_5)_3$; generation of 1. In a typical experiment, a septum screw-capped NMR tube was charged with 3 mg of (NN)$PtMe_2$ (6 μmol) and 7 mg of $B(C_6F_5)_3$ (14 μmol, 2.3 equiv). Dry, degassed CF_3CD_2OD (0.6 ml) was then added with a syringe. The NMR tube was then closed and shaken to mix the reagents. The red platinum complex dissolved with reaction, liberating methane and affording an orange solution. A 1H NMR spectrum showed clean production of the platinum cation, **1**, along with the formation of methane. Notably, both CH_4 and CH_3D were observed by ^{1}H NMR, as were the corresponding $[Pt–CH_3]^+$ and $[Pt–CH_2D]^+$ resonances. By integration, the ratio of $[Pt–CH_3]^+$ and $[Pt–CH_2D]^+$ appeared to be ca. 1 to 1. ^{1}H NMR (600 MHz, CF_3CD_2OD) δ / ppm: 0.15 (t, C*H*$_3$D, $^2J_{HD}$ = 2 Hz); 0.16 (s, C*H*$_4$); 0.76 (bs, Pt–C*H*$_2$D); 0.77 (bs, Pt–C*H*$_3$); 1.84 (s, N=C–C*H*$_3$, 3H); 1.99 (s, N=C–C*H*$_3$, 3H); 2.34 (s, Ar–C*H*$_3$, 6H); 2.36 (s, Ar–C*H*$_3$, 6H); 6.59 (s, *o*-Ar*H*, 2H); 6.77 (s, *o*-Ar*H*, 2H); 7.04 (s, *p*-Ar*H*, 1H); 7.09 (s, *p*-Ar*H*, 1H). Supporting evidence of a protonolytic path to **1** can be observed in ^{1}H and ^{19}F NMR spectra of CD_2Cl_2 solutions containing $B(C_6F_5)_3$ and CF_3CH_2OH. Notably, addition of 5 equiv of CF_3CH_2OH to a CD_2Cl_2 solution of $B(C_6F_5)_3$ results in the appearance of a downfield, "acidic" proton resonance that is in chemical exchange with the upfield hydroxylic proton of CF_3CH_2OH (all signals associated with the trifluoroethanol group are broad). ^{1}H NMR (300 MHz, CD_2Cl_2) δ / ppm: 2.43 (CF_3CH_2O*H*); 3.97 (CF_3C*H*$_2$OH/CF_3C*H*$_2$O(H)B(C_6F_5)$_3$); 8.30 (CF_3CH_2O(*H*)B(C_6F_5)$_3$). ^{19}F NMR (282 MHz, CD_2Cl_2) δ / ppm: –77.8 (s, C*F*$_3$CH$_2$O–); –134.5 (bs, *o*-Ar*F*); –154.3 (bs, *p*-Ar*F*); –163.4 (s, *m*-Ar*F*).

Kinetic Experiments. A solution of the platinum cation, **1**, was generated as above. An initial ^{1}H NMR spectrum was acquired to confirm complete and clean formation of **1**. A

microsyringe was used to add 10 μl of C_6H_6 (0.11 mmol) through the septum; the solution was briefly shaken and inserted into the NMR probe, which had come to an equilibrium temperature of 24 °C. After briefly shimming on the sample, an array of 30 spectra was acquired over 60 minutes. After completion of the run, a solution height (h) of 46 mm was measured and used to calculate a total sample volume of 0.63 ml (V/ml = 0.01384h – 0.006754). The intensity data for relating the concentrations of reagent **1** and product **2** were obtained from the NMR spectra and were fit to the first-order exponential equations

$$[1] = Ae^{-k_{obs}t}, \text{ and}$$
$$[2] = A(1 - e^{-k_{obs}t}).$$

Second-order rate constants were obtained from a plot of k(obs) vs $[C_6H_6]$ over the concentration range 0.1 to 0.5 M. Whereas the mesitylene reactions were treated analogously, in the case of *para*-xylene a more elaborate data work-up was necessary. An accurate recording of t_0 (the point at which the Pt cation and *p*-xylene were mixed) was necessary because of the competing reactions. Additionally, the integration of peaks associated with **1**, **4a**, and **4b** had to be normalized in order to accurately measure k_{Ar}(obs) and k_{Bz}(obs). After normalization and adjustment to t_0, [**1**], [**4a**], and [**4b**] were fit to the equations

$$[1] = Ae^{-k't}; k' = k_{Ar} + k_{Bz}$$
$$[4a] = \frac{Ak_{Ar}}{k_{isom} - k'}\left(e^{-k't} - e^{-k_{isom}t}\right)$$
$$[4b] = A\left\{1 - e^{-k't} - \frac{k_{Ar}}{k_{isom} - k'}\left(e^{-k't} - e^{-k_{isom}t}\right)\right\}$$

At completion of each reaction, a final ^{1}H NMR spectrum was recorded. An aliquot of CD_3CN (ca. 10 equiv) was then added to the NMR tube by syringe and the ^{1}H NMR spectrum of the $[(NN)Pt(R)(NCCD_3)]^+$ cation was recorded. ^{1}H NMR data for cations **1-4**, and ^{13}C NMR data for **1** and **4b**, are given in Tables S1 and S2 respectively.

Table S1. ^{1}H NMR data (600 MHz) for $[(NN)Pt(R)(L)]^+$ cations in CF_3CD_2OD ((NN) = Ar–N=C(Me)–C(Me)=N–Ar, Ar=3,5-$C_6H_4Me_2$; [Pt] ≈ 0.012 M; [R–H] ≈ 0.15 M).

Cation	Assignment	δ / ppm L = CF_3CD_2OD	δ / ppm L = CD_3CN
$[(NN)PtMe(L)]^+$	Pt–C*H*$_3$	0.76; 0.77[a,b]	0.65; 0.66[a,b]
1	–N=CC*H*$_3$	1.84; 1.99	1.95; 2.02
	(NN) *m*-ArC*H*$_3$	2.34; 2.36	2.34; 2.36
	(NN) *o*-Ar*H*	6.59; 6.77	6.56; 6.71
	(NN) *p*-Ar*H*	7.04; 7.09	7.03; 7.07
$[(NN)PtPh(L)]^+$	–N=CC*H*$_3$	1.93; 2.11	2.07; 2.14
2	(NN) *m*-ArC*H*$_3$	2.09; 2.38	2.09; 2.39
	(NN) *o*-Ar*H*	6.31; 6.84	6.27; 6.77
	(NN) *p*-Ar*H*	6.67; 7.12	6.71; 7.10
	(Ph) *o*-Ar*H*	6.85 (d, 5.6 Hz)	6.78 (d, 8.3 Hz)
	(Ph) *m*-Ar*H*	6.74 (t, 7.4 Hz)	6.72 (t, 7 Hz)
	(Ph) *p*-Ar*H*	6.66 (t, 8.3 Hz)	6.68 (t, 7 Hz)
$[(NN)Pt(CH_2C_6H_3Me_2)(L)]^+$	Pt–C*H*$_2$Ar	2.51[a]	2.86[a]
3	–N=CC*H*$_3$	1.91; 1.96[c]	1.95; 2.01
	(NN) *m*-ArC*H*$_3$	2.33; 2.37	2.34; 2.38
	(NN) *o*-Ar*H*	6.05; 6.76	6.46; 6.64
	(NN) *p*-Ar*H*	7.00; 7.05	7.04; 7.10
	(Bz) *m*-ArC*H*$_3$	1.96[c]	2.15
	(Bz) *o*-Ar*H*	5.96	6.65
	(Bz) *p*-Ar*H*	6.89	6.67
$[(NN)Pt(C_6H_4Me_2)(L)]^+$	–N=CC*H*$_3$	1.89; 2.13	2.04; 2.13
4a	(NN) *m*-ArC*H*$_3$	2.09, 2.47;[d] 2.38	2.01, 2.36;[d] 2.39
	(NN) *o*-Ar*H*	6.30, 6.35;[d] 6.86	6.15, 6.35;[d] 6.78[c]
	(NN) *p*-Ar*H*	6.67; 7.13	6.78[c] ; 7.10
	(Ar) ArC*H*$_3$	2.05; 2.08	1.98; 2.18
	(Ar) *3*-Ar*H*	6.52 (d, 7.4 Hz)	6.58 (d, 7.4 Hz)
	(Ar) *4*-Ar*H*	6.44 (d, 7.4 Hz)	6.44 (d, 7.2 Hz)
	(Ar) *6*-Ar*H*	6.77	6.67
$[(NN)Pt(CH_2C_6H_4Me)(L)]^+$	Pt–C*H*$_2$Ar	2.61[a]	2.87[a]
4b	–N=CC*H*$_3$	1.92, 2.00	1.94; 2.01
	(NN) *m*-ArC*H*$_3$	2.36; 2.39	2.37; 2.40
	(NN) *o*-Ar*H*	6.27; 6.76	6.46, 6.64
	(NN) *p*-Ar*H*	7.05; 7.17	7.03; 7.15
	(Bz) *p*-ArC*H*$_3$	1.78	2.10
	(Bz) *o*-Ar*H*	6.26 (d, 7 Hz)	6.71 (d, 7.8 Hz)
	(Bz) *m*-Ar*H*	6.53 (d, 7 Hz)	6.84 (d, 7.8 Hz)

[a] J_{PtH} coupling constants were not well-resolved at high magnetic field. [b] The first resonance is for the Pt–C*H*$_2$D isotopomer. [c] Overlapping resonances. [d] The *para*-xylyl isomer displays hindered rotation about both the Pt–(*para*-xylyl) bond and the neighboring N–(aryl) bond of the diimine ligand. Thus, the *o*-*H* and *m*-C*H*$_3$ resonances of the aryl imine proximate to the *para*-xylyl group are split in the ^{1}H NMR spectrum.

Table S1 (cont.). ^{1}H NMR data (600 MHz) for $[(NN)Pt(R)(L)]^+$ cations in CF_3CD_2OD ((NN) = Ar–N=C(Me)–C(Me)=N–Ar, Ar=3,5-$C_6H_4Me_2$; [Pt] ≈ 0.012 M; [R–H] ≈ 0.15 M).

Cation	Assignment	δ / ppm L = CF_3CD_2OD	δ / ppm L = CD_3CN
$[(NN)Pt(CH_2(Me)C_6H_4Et)(L)]^+$	Pt–CH_2(Me)Ar	2.81 (q, J = 6.6 Hz;[a] J_{PtH} = 40 Hz)[b]	2.60 (q, J = 7.2 Hz)[a]
5	Pt–CH_2(CH_3)Ar	0.37 (d, J = 6.6 Hz)	1.04 (d, J = 7.2 Hz)
	–N=CCH_3	2.01; 2.07	2.01, 2.05
	(NN) m-ArCH_3	2.09; 2.22; 2.30; 2.31	2.26, 2.29, 2.35, 2.41
	(NN) o-ArH and p-ArH	6.68; 6.80; 6.82; 6.84 7.06; 7.13	Indistinguishable[c]
	(Bz) p-ArCH_2Me	2.15 (m); 2.17 (m)	2.48 (q, J = 7.8 Hz)
	(Bz) p-ArCH_2CH_3	0.99 (t, J = 7.2 Hz)	1.14 (t, J = 7.8 Hz)
	(Bz) o-ArH	5.86 (d, J = 7.0 Hz; J_{PtH} = 23 Hz)[b]	Indistinguishable[c,d]
	(Bz) o-ArH	6.27 (d J = 7.0 Hz)	Indistinguishable[c,d]
	(Bz) m-ArH	6.10 (br s); 6.73 (br s)	Indistinguishable[c]

[a] J_{PtH} coupling constants were not well-resolved at high magnetic field. [b] $^2J_{PtH}$ coupling constant reported at 300 MHz. [c] The aryl region of the reaction mixture contained many overlapping peaks between 6.4 and 7.2 ppm. [d] The upfield (Bz)-ArH resonances moved downfield with the addition of CD_3CN and analysis at 300 MHz did not reveal any characteristic PtH coupling suggesting η^1-bonding.

Table S2. ^{1}H NMR data (600 MHz) for $[(NN)Pt(R)(L)]^+$ cations in CF_3CD_2OD ((NN) = Mes–N=C(Me)–C(Me)=N–Mes [Pt] ≈ 0.012 M; [R–H] ≈ 0.15 M).

Cation	Assignment	δ / ppm L = CF_3CD_2OD	δ / ppm L = CD_3CN
$[(NN)PtMe(L)]^+$	Pt–CH_3	0.64; 0.62[a,b]	0.49; 0.50[a,b]
s1	–N=CCH_3	1.74; 1.89	1.88; 1.94
	(NN) o-ArCH_3 and p-ArCH_3	2.14; 2.27; 2.291; 2.304	2.13; 2.32; 2.31; 2.33
	(NN) m-ArH	7.02; 7.08	7.04; 7.09
$[(NN)Pt(CH_2(Me)C_6H_4Et)(L)]^+$	Pt–CH_2(Me)Ar	2.76 (q, J = 6.6 Hz;[a] J_{PtH} = 33 Hz)[c]	2.46 (q, J = 7.2 Hz)[a]
s2	Pt–CH_2(CH_3)Ar	0.32 (d, J = 6.6 Hz)	1.01 (d, J = 6.9 Hz)
	–N=CCH_3	1.85; 1.89	1.88; 1.94
	(NN) o-ArCH_3 and p-ArCH_3	1.46; 1.96; 2.18; 2.34 (2); 2.37	2.02; 2.09; 2.22; 2.26; 2.30; 2.34
	(NN) m-ArH	6.91; 7.06; 7.12; 7.13	6.90; 7.01; 7.06; 7.08
	(Bz) p-ArCH_2Me	2.07 (m); 2.16 (m)	Obscured
	(Bz) p-ArCH_2CH_3	1.03 (t, J = 7.2 Hz)	1.12 (t, J = 7.5 Hz)
	(Bz) o-ArH	5.62 (d, J = 6.0 Hz; J_{PtH} = 23 Hz)[c]	6.74 (d, J = 8.1 Hz)
	(Bz) o-ArH	6.05 (d, J = 5.8 Hz)	
	(Bz) m-ArH	6.96 (AB splitting)	6.90 (d, J = 8.1 Hz)

[a] J_{PtH} coupling constants were not well-resolved at high magnetic field. [b] The first resonance is for the Pt–CH_2D isotopomer. [c] $^2J_{PtH}$ coupling constant reported at 300 MHz.

Table S3. ^{13}C NMR data for $[(NN)Pt(R)(L)]^+$ cations in CF_3CD_2OD ([Pt] ≈ 0.012 M; [R–H] ≈ 0.15 M).

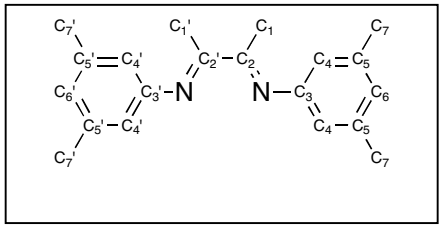

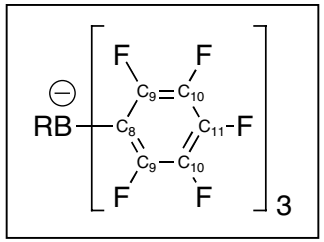

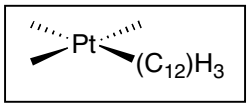

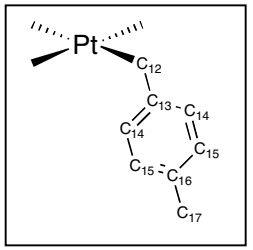

		Free Ligand	$(NN)PtMe_2$	$[(NN)PtMe(solv)][BR_4]$	$[(NN)PtMe(NCMe)][BR_4]$	$[(NN)PtBz(solv)][BR_4]$	$[(NN)PtBz(NCMe)][BR_4]$
diimine ligand	C1	15.6	21.0	20.8	20.8	20-23	20-24
	C1'	~	~	22.2	22.2	~	~
	C2	168.2	170.4	174.5	174.7	178.2	175.4
	C2'	~	~	183.5	184.4	179.2	184.1
	C3	151.2	147.5	146.8	146.6	147.9	146.6
	C3'	~	~	148.3	147.0	150.5	146.7
	C4	116.5	119.4	119-122	119-122	118-121	119-122
	C4'	~	~	~	~	~	~
	C5	138.8	138.7	142.0	141.9	142.1	142.0
	C5'	~	~	142.6	142.0	142.4	142.3
	C6	125.5	128.0	not obs	not obs	128-132	128-131
	C6'	~	~	not obs	not obs	~	~
	C7	21.6	21.6	21.4	21.5 (br)	20-23	20-24
	C7'	~	~	21.5	~	~	~
borate	C8	~	~	not obs	not obs	not obs	not obs
	C9	~	~	150.1 (240 Hz)	150.1 (239 Hz)	150.2 (242 Hz)	150.2 (239 Hz)
	C10	~	~	139.0 (247 Hz)	138.7 (250 Hz)	not res	not res
	C11	~	~	141.6 (245 Hz)	140.9 (240 Hz)	not res	not res
Pt-R	C12	~	–13.8 (791 Hz)	21.5 (207 Hz)	21.4 (204 Hz)	33.5	not obs
	C13	~	~	~	~	151.1	149.4
	C14	~	~	~	~	128-132	128-131
	C15	~	~	~	~	139.9	139.9
	C16	~	~	~	~	128-132	128-131
	C17	~	~	~	~	20-23	20-24

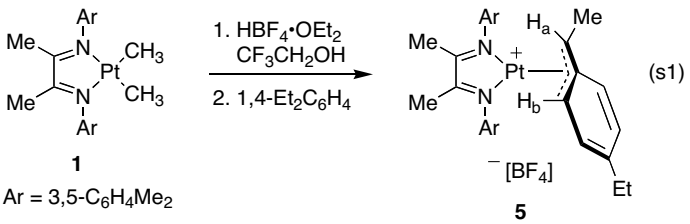

Platinum η^3-complex 5 (eq s1). To a suspension of (NN)$PtMe_2$ (**1**, NN = Ar-N=C(Me)-C(Me)=N-Ar, Ar = 3,5-$C_6H_4Me_2$) (0.100 g, 0.193 mmol) in 8 mL CF_3CH_2OH was added 0.037 mL of a 54 wt% solution of HBF_4 in Et_2O (0.23 mmol). Upon homogeneity, 0.120 mL of 1,4-diethylbenzene (0.772 mmol) was added to the reaction solution. After 20 h, the reaction mixture was concentrated *in vacuo* to afford a red viscous oil (extensive decomposition occurred upon evaporation to dryness): ^{1}H NMR (600 MHz, CD_2Cl_2) δ 7.08 (s, 1H), 7.07 (s, 1H), 7.02 (s, 1H), 6.93 (s, 1H), 6.91 (s, 1H), 6.67 (br s, 1H), 6.46 (s, 1H), 6.23 (d, J = 7.2 Hz, 1H), 6.02 (br s, 1H), 5.87 (dd, J = 1.5, 7.2 Hz, J_{PtH} = 22 Hz, 1H), 2.87 (q, J = 6.6 Hz, J_{PtH} = 30 Hz, 1H), 2.40 (s, 3H), 2.32 (s, 3H), 2.27 (s, 3H), 2.07 (m, 2H),[a] 1.99 (s, 3H), 1.95 (s, 3H), 1.92 (s, 3H), 0.99 (t, J = 7.2 Hz, 3H), 0.37 (d, J = 6.6 Hz, 3H); ^{13}C NMR (125 MHz, CF_3CD_2OD) δ 183.0, 182.6, 149, 148, 145, 144, 143.6, 143.1, 142.9, 142.7, 137, 136, 134, 133, 132, 131, 129, 121, 120, 114, 43, 30, 21.7, 21.5, 19.9, 19.7, 19.6, 19.5, 14.3, 13; HRMS (FAB) m / z calcd for $C_{30}H_{37}N_2Pt^+$ $(M–BF_4)^+$ 620.2605, found 620.2575.

[a]Identified using 2D NMR COSY experiment.

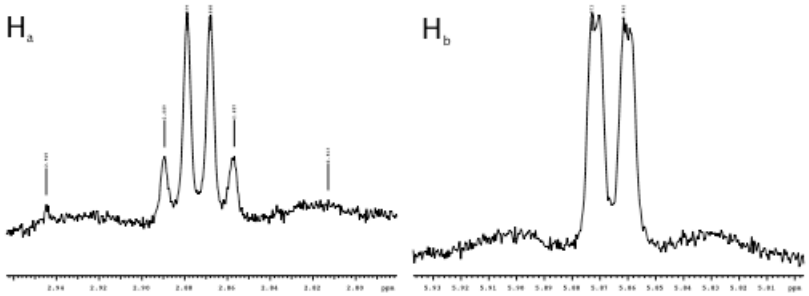

Figure s1. Diagnostic ^{1}H NMR peaks

Platinum η^3-complex s2 (eq s2). To a suspension of (NN)$PtMe_2$ (**s1**, NN = Mes-N=C(Me)-C(Me)=N-Mes) (0.092 g, 0.15 mmol) in 8 mL CF_3CH_2OH was added 0.032 mL of a 54 wt% solution of HBF_4 in Et_2O (0.19 mmol). Upon homogeneity, 0.065 mL of 1,4-diethylbenzene (0.42 mmol) was added to the reaction solution. After 6 d at 25 °C, the reaction mixture was warmed to 45 °C. After 18h, the reaction mixture was cooled to 25 °C and was concentrated *in vacuo*. The resulting red residue was re-dissolved in 5 mL of methanol and concentrated *in vacuo* to afford 0.180 g of a dark red residue: ^{1}H NMR (600 MHz, CD_2Cl_2) δ 7.11 (s, 1H), 7.10 (s, 1H), 7.04 (s, 1H), 6.92 (s, 1H), 6.91 (s, 1H), 6.90 (s, 1H), 5.99 (d, J = 6.0 Hz, 1H), 5.63 (dd, J = 7.0, 1.8 Hz, J_{PtH} = 19 Hz, 1H), 2.75 (q, J = 6.6 Hz, J_{PtH} = 24 Hz, 1H), 2.39 (s, 3H), 2.37 (s, 3H), 2.36 (s, 3H), 2.21 (s, 3H), 2.14 (m, 1H),[a] 2.45 (m, 1H),[a] 2.01 (s, 3H), 1.98 (s, 3H), 1.97 (s, 3H), 1.46 (s, 3H), 1.03 (t, J = 7.8 Hz, 3H), 0.30 (d, J = 6.6 Hz, 3H); ^{13}C NMR (150.8 MHz, CD_2Cl_2) δ 180, 177, 143.4, 143.2, 141, 140.7, 140, 138, 135.0, 134.9, 130.22, 130.15, 129.9, 129.8, 129.7,

129, 128, 127, 116 (b), 112, 42, 29, 19.5, 19.3, 18.8, 18, 17.73, 17.68, 17.3, 16.7, 14, 12; IR (KBr pellet) 2968, 1610, 1386, 1059, 851 cm^{-1}; HRMS (FAB) *m* / *z* calcd for $C_{32}H_{41}N_2Pt^+$ $(M–BF_4)^+$ 648.2918, found 648.2932.

[a]Identified using 2D NMR COSY experiment.

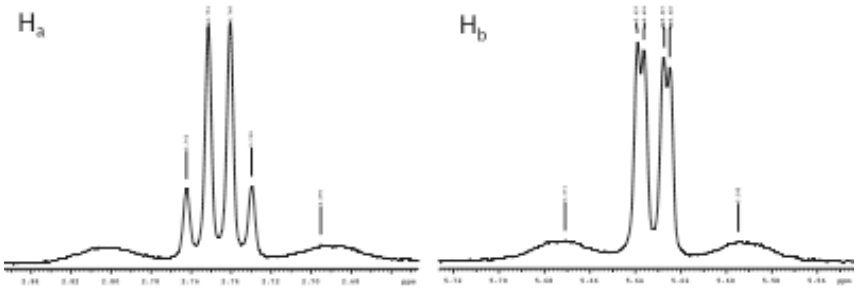

Figure s2. Diagnostic ^1H NMR peaks

Suggested Mechanistic Interpretations.

1. Kinetic Isotope Effects

Previously we reported that the KIE for benzene activation by complexes analogous to **1** depends upon the steric bulk of the NN ligand: for more crowded ligands (those with 2,6-dimethylaryl groups) there is very little or no isotope effect, whereas for less crowded ligands there is typically an isotope effect around 2. The interpretation is based on a switch in rate-determining step: for the less crowded case the actual C-H bond breaking step ($Z^{\ddagger}$) is rate-determining, but the more sterically demanding ligands raise the energy of the transition state for entry of benzene into the coordination sphere ($Y^{\ddagger}$), via solvent-assisted associative displacement of water to form a π-benzene complex, which thus becomes rate-determining. Figure S3 represents the two cases.

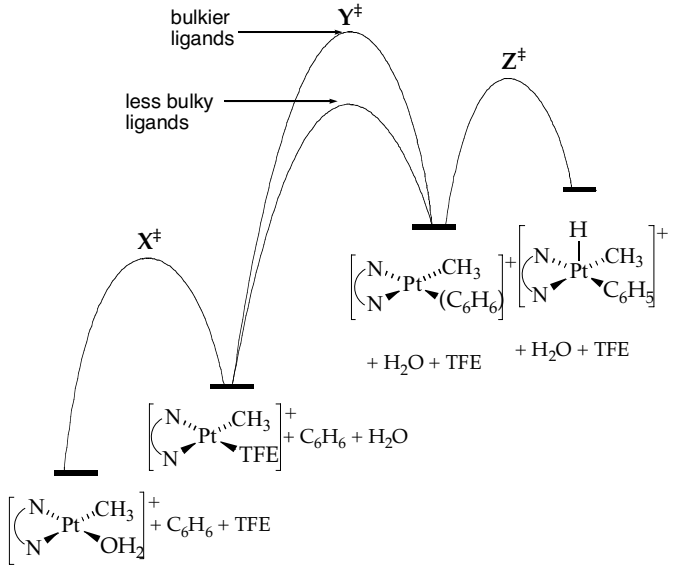

Figure s3. Energy Diagram for Benzene Reaction with Complexes of More- and Less-Crowded Ligands.

As **1** contains a non-bulky ligand, the observation of KIE ~ 2 for aromatic activation is consistent; but there is essentially no KIE for activation at the benzylic position? This suggests that the replacement of solvent by hydrocarbon remains rate-determining even for this less-crowded case. Why should that be so? Note that this process leads to a π complex for aromatic activation, but a σ complex for benzylic activation. The latter is expected to be considerably less stable, and the transition state leading to it should therefore be correspondingly higher in energy. It is not unreasonable to suppose that effect could push $Y^{‡}$ back above $Z^{‡}$ (Figure s4).

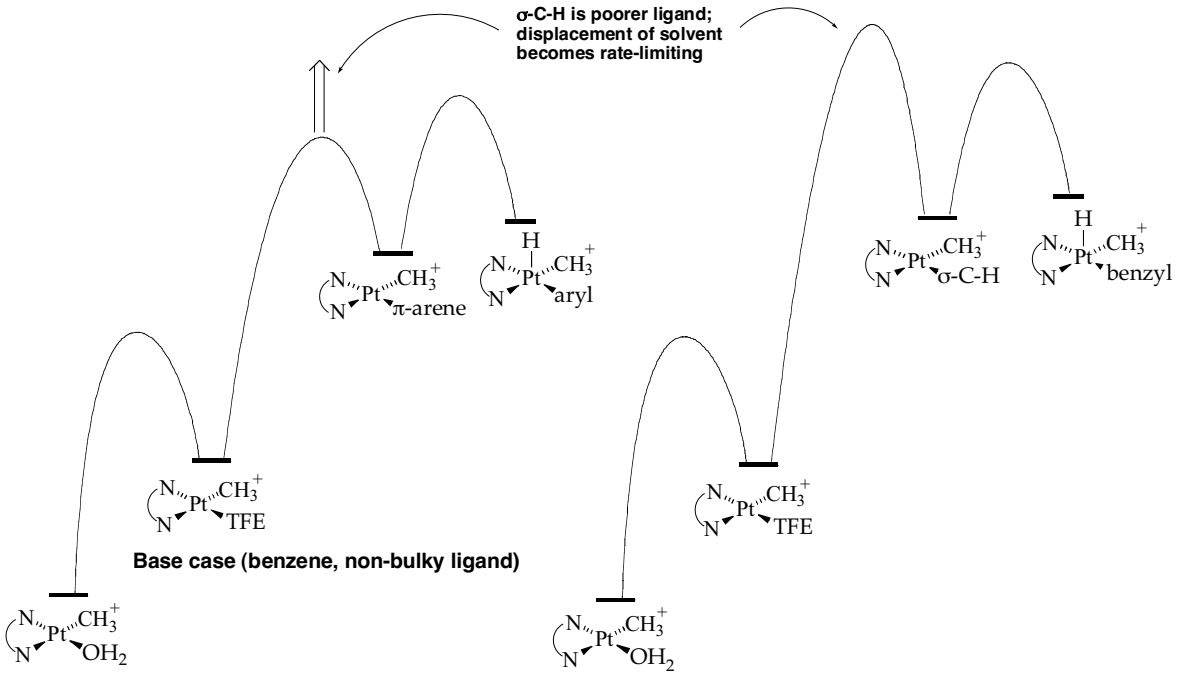

Figure s4. KIE Explanation

2. Relative Reactivities

The relative rates of benzylic vs. aromatic activation of *p*-xylene by a complex very similar to **1** (differing only in 3,5-alkyl substituents on the ligand) are at least 10:1 when water is present, but only about 2:1 in the current anhydrous system. (The numbers in Table 1 of the main text have large uncertainties, as a consequence of the fitting procedure, but it is apparent from Figure 1 that the ratio is much less than 10:1.) According to the mechanism represented by Figure S1 there is no reason why there should be any difference, whether water is present or not. A (hopefully) plausible explanation can be generated by introducing a direct (rather than solvent-assisted) component for displacement of water by *p*-xylene. The dependence of rate on water concentration for the benzene case ruled out the possibility of any significant contribution from the direct pathway; but *p*-xylene is expected to be a better donor than benzene, and could thereby become a sufficiently more potent nucleophile to allow the direct route to compete. In that case, although the relative rates for aromatic vs. benzylic activation following the solvent-assisted path would still be the same whether water was present or not, there would be an additional contribution to the aromatic activation, but not the benzylic activation, in the presence of water. This model is represented in Figure s5.

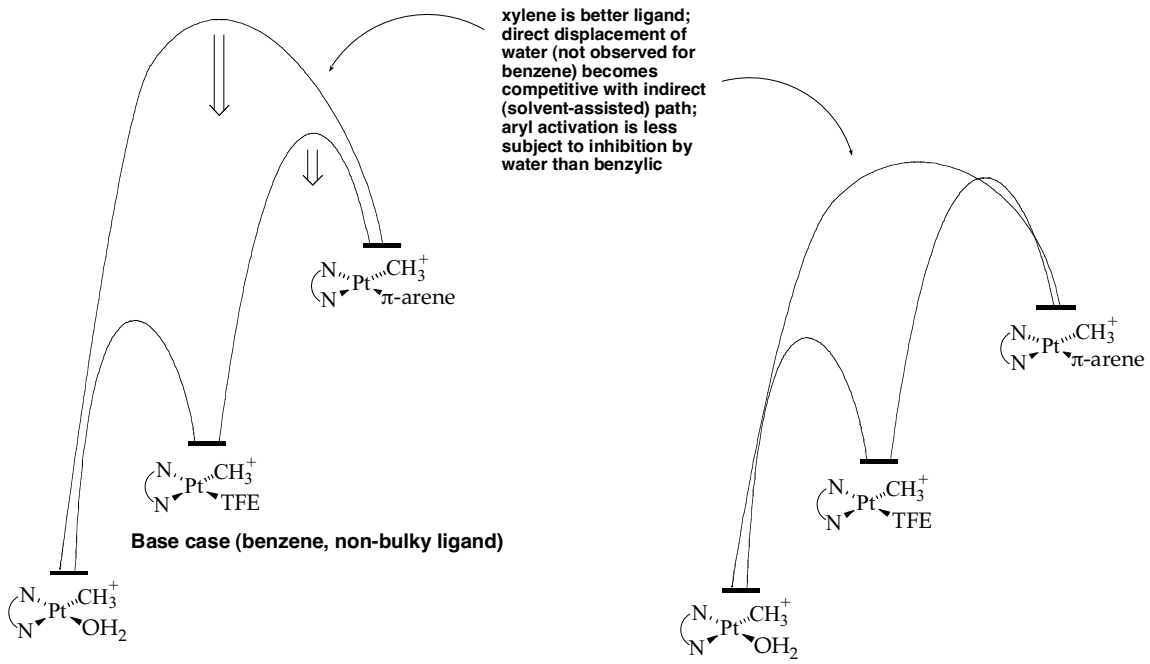

Figure s5. Relative Rate Explanation

General Details of X-Ray Data Collection and Reduction. X-ray diffraction data were collected on a Siemens 3-circle platform diffractometer equipped with a CCD detector. Measurements were carried out at 98 K using Mo Kα (λ = 0.71073 Å) radiation, which was wavelength selected with a single crystal graphite monochromator. Four sets of data were collected using ω scans and a –0.3° scan width. The data frames were integrated to *hkl*/intensity and final unit cells were calculated by using the SAINT program v.6.02 from Bruker AXS. The structures were solved and refined with the SHELXTL v6.12 suite of programs developed by G. M. Sheldrick and Bruker AXS, 2000.

X-ray Structure of [(NN)Pt(*para*-$CH_2C_6H_4Me$)(NCMe)][BF_4] (4b'). X-ray quality crystals of **4b'** were obtained by the following procedure. **1** was prepared from (NN)$PtMe_2$ and an aliquot of HBF_4/Et_2O in CF_3CH_2OD. *para*-Xylene was added and the solution was stirred at room temperature overnight. A few drops of MeCN was added to the solution and the volatiles were removed *in vacuo*. The resulting solid residue was taken up in a minimal volume of MeCN and diethyl ether was added by vapor diffusion, causing the deposition of red crystals. A 0.24 mm _ 0.16 mm _ 0.08 mm, red plate crystal was mounted on a glass fiber using Paratone N. A total of 28210 reflections were collected in the θ range of 1.99° to 23.24°, of which 3076 were unique (R_{int} = 0.0581). The structure was solved by the Patterson heavy atom method in conjunction with standard difference Fourier techniques. A single carbon atom (C9) was refined isotropically. Hydrogen atoms were placed in calculated positions using a standard riding model and they were refined isotropically. An empirical absorption correction was applied to the data using XPREP. The largest peak and hole in the difference map were 0.945 eÅ^{-3} and –1.144 eÅ^{-3}, respectively. The least squares refinement converged normally giving residuals of *R1* = 0.0295, *wR2* = 0.0628, and GOF = 1.227. The crystal data for $C_{15}H_{18}B_{0.5}F_2N_{1.5}Pt_{0.5}$: tetragonal, P4(3)2(1)2, *Z* = 16, *a* = 10.4025(12) Å, *b* = 10.4025(12) Å, *c* = 55.489(9) Å, *V* = 6004.6(13) Å^3, ρ_{calc} = 1.594 g/cm^3, F(000) = 2848.

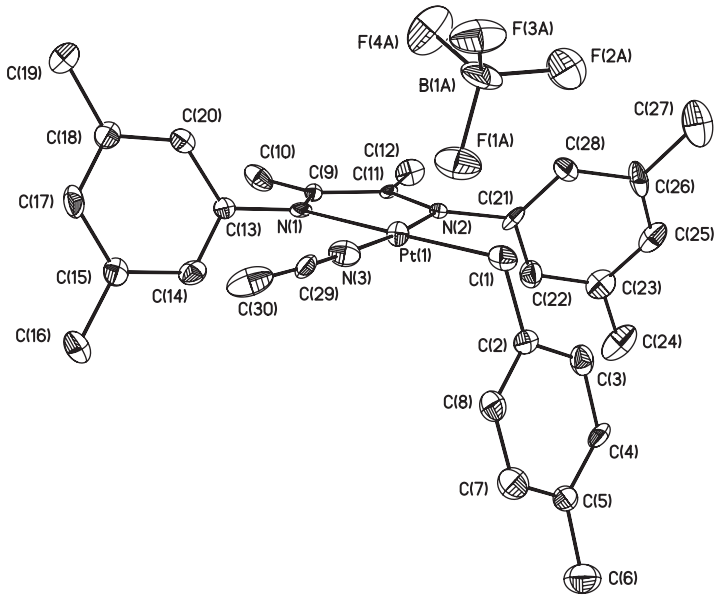

Table S4. Crystal data and structure refinement for **4b'**.

Identification code	afh030m	
Empirical formula	C15 H18 B0.50 F2 N1.50 Pt0.50	
Formula weight	360.26	
Temperature	98(2) K	
Wavelength	0.71073 Å	
Crystal system	Tetragonal	
Space group	P4(3)2(1)2	
Unit cell dimensions	a = 10.4025(12) Å	α = 90°
	b = 10.4025(12) Å	β = 90°
	c = 55.489(9) Å	γ= 90°
Volume	6004.6(13) Å^3	
Z	16	
Density (calculated)	1.594 Mg/m^3	
Absorption coefficient	4.722 mm^{-1}	
F(000)	2848	
Crystal size	0.24 x 0.16 x 0.08 mm^3	
θ range for data collection	1.99 to 23.24°	
Index ranges	$-9 \le h \le 8$, $-9 \le k \le 9$, $-50 \le l \le 61$	
Reflections collected	28764	
Independent reflections	3076 [R(int) = 0.0581]	
Completeness to θ = 23.24°	74.5 %	
Absorption correction	Empirical	
Refinement method	Full-matrix least-squares on F^2	
Data / restraints / parameters	3076 / 0 / 356	
Goodness-of-fit on F^2	1.227	
Final R indices [I>2_(I)]	R1 = 0.0295, wR2 = 0.0628	
R indices (all data)	R1 = 0.0318, wR2 = 0.0634	
Absolute structure parameter	0.001(12)	
Extinction coefficient	0.00000(5)	
Largest diff. peak and hole	0.945 eÅ^{-3}, –1.144 eÅ^{-3}	

Table S5. Atomic coordinates (x 10^4) and equivalent isotropic displacement parameters ($Å^2$ x 10^3)for **4b'**. U(eq) is defined as one third of the trace of the orthogonalized U_{ij} tensor.

	x	y	z	U(eq)
Pt(1)	4835(1)	4106(1)	3909(1)	17(1)
N(1)	5602(6)	2948(6)	3635(1)	13(2)
N(2)	6072(6)	2966(6)	4092(1)	13(2)
N(3)	3726(7)	5145(7)	3704(1)	23(2)
C(1)	4131(8)	5198(8)	4195(1)	18(2)
C(2)	3028(9)	4553(8)	4317(1)	17(2)
C(3)	3210(9)	3908(9)	4539(1)	25(2)
C(4)	2199(9)	3248(9)	4647(1)	24(2)
C(5)	988(10)	3199(9)	4543(1)	26(2)
C(6)	-63(9)	2407(10)	4657(2)	39(3)
C(7)	810(10)	3887(9)	4333(1)	31(3)
C(8)	1801(9)	4544(9)	4221(1)	25(2)
C(9)	6459(8)	2126(8)	3698(1)	11(2)
C(10)	7103(9)	1173(8)	3534(1)	27(2)
C(11)	6744(7)	2174(8)	3950(1)	10(2)
C(12)	7750(8)	1276(8)	4060(1)	23(2)
C(13)	5287(9)	3090(8)	3383(1)	19(2)
C(14)	4017(9)	3005(8)	3309(1)	20(2)
C(15)	3671(9)	3218(8)	3069(1)	22(2)
C(16)	2287(9)	3061(10)	2987(1)	34(3)
C(17)	4628(10)	3574(8)	2906(1)	25(2)
C(18)	5915(10)	3687(8)	2977(1)	24(2)
C(19)	6964(9)	4108(10)	2806(1)	38(3)
C(20)	6233(8)	3431(8)	3217(1)	19(2)
C(21)	6207(8)	2962(9)	4348(1)	17(2)
C(22)	5734(9)	1928(9)	4476(1)	25(2)
C(23)	5794(9)	1911(9)	4726(1)	27(2)
C(24)	5252(10)	832(10)	4872(1)	42(3)
C(25)	6355(8)	2966(10)	4840(1)	28(3)
C(26)	6856(8)	4007(10)	4713(1)	28(2)
C(27)	7482(11)	5127(10)	4833(2)	51(3)
C(28)	6779(8)	3990(9)	4462(1)	23(2)
C(29)	3079(8)	5673(8)	3574(1)	17(2)
C(30)	2289(9)	6377(8)	3396(2)	30(3)
B(1A)	5047(11)	8878(11)	3910(2)	35(3)
F(1A)	3904(5)	8189(5)	3890(1)	37(1)
F(2A)	5401(5)	8966(6)	4148(1)	59(2)
F(3A)	4820(5)	10144(5)	3828(1)	42(1)
F(4A)	6023(6)	8343(5)	3778(1)	46(2)

Table S6. Bond lengths [Å] and angles [°] for **4b'**.

Pt(1)-N(3)	1.949(8)	C(13)-C(20)	1.394(11)
Pt(1)-N(2)	2.022(6)	C(14)-C(15)	1.396(10)
Pt(1)-C(1)	2.082(7)	C(15)-C(17)	1.393(11)
Pt(1)-N(1)	2.101(6)	C(15)-C(16)	1.518(12)
N(1)-C(9)	1.285(9)	C(17)-C(18)	1.400(13)
N(1)-C(13)	1.443(10)	C(18)-C(20)	1.394(10)
N(2)-C(11)	1.338(9)	C(18)-C(19)	1.511(12)
N(2)-C(21)	1.428(8)	C(21)-C(28)	1.375(12)
N(3)-C(29)	1.130(9)	C(21)-C(22)	1.379(12)
C(1)-C(2)	1.492(11)	C(22)-C(23)	1.392(11)
C(2)-C(8)	1.383(12)	C(23)-C(25)	1.393(13)
C(2)-C(3)	1.415(11)	C(23)-C(24)	1.493(12)
C(3)-C(4)	1.390(12)	C(25)-C(26)	1.391(13)
C(4)-C(5)	1.388(12)	C(26)-C(28)	1.400(10)
C(5)-C(7)	1.379(11)	C(26)-C(27)	1.492(13)
C(5)-C(6)	1.510(13)	C(29)-C(30)	1.478(12)
C(7)-C(8)	1.383(12)	B(1A)-F(4A)	1.371(12)
C(9)-C(11)	1.427(9)	B(1A)-F(2A)	1.376(12)
C(9)-C(10)	1.504(11)	B(1A)-F(1A)	1.393(12)
C(11)-C(12)	1.530(10)	B(1A)-F(3A)	1.414(13)
C(13)-C(14)	1.386(12)		

N(3)-Pt(1)-N(2)	174.3(2)	C(14)-C(13)-N(1)	119.7(7)
N(3)-Pt(1)-C(1)	86.2(3)	C(20)-C(13)-N(1)	120.4(8)
N(2)-Pt(1)-C(1)	99.4(3)	C(13)-C(14)-C(15)	121.1(8)
N(3)-Pt(1)-N(1)	96.8(3)	C(17)-C(15)-C(14)	118.4(8)
N(2)-Pt(1)-N(1)	77.7(2)	C(17)-C(15)-C(16)	120.8(7)
C(1)-Pt(1)-N(1)	177.0(3)	C(14)-C(15)-C(16)	120.8(8)
C(9)-N(1)-C(13)	119.5(6)	C(15)-C(17)-C(18)	121.6(7)
C(9)-N(1)-Pt(1)	116.4(5)	C(20)-C(18)-C(17)	118.5(8)
C(13)-N(1)-Pt(1)	123.9(5)	C(20)-C(18)-C(19)	118.9(9)
C(11)-N(2)-C(21)	122.2(6)	C(17)-C(18)-C(19)	122.6(7)
C(11)-N(2)-Pt(1)	113.5(4)	C(18)-C(20)-C(13)	120.7(8)
C(21)-N(2)-Pt(1)	124.3(5)	C(28)-C(21)-C(22)	121.7(7)
C(29)-N(3)-Pt(1)	175.0(7)	C(28)-C(21)-N(2)	119.7(8)
C(2)-C(1)-Pt(1)	111.8(5)	C(22)-C(21)-N(2)	118.5(8)
C(8)-C(2)-C(3)	117.1(8)	C(21)-C(22)-C(23)	120.4(8)
C(8)-C(2)-C(1)	122.5(7)	C(22)-C(23)-C(25)	117.4(8)
C(3)-C(2)-C(1)	120.4(8)	C(22)-C(23)-C(24)	122.2(9)
C(4)-C(3)-C(2)	120.5(8)	C(25)-C(23)-C(24)	120.4(8)
C(5)-C(4)-C(3)	121.7(8)	C(26)-C(25)-C(23)	122.9(7)
C(7)-C(5)-C(4)	117.0(9)	C(25)-C(26)-C(28)	118.1(9)
C(7)-C(5)-C(6)	122.9(9)	C(25)-C(26)-C(27)	123.2(7)
C(4)-C(5)-C(6)	120.1(8)	C(28)-C(26)-C(27)	118.7(10)
C(5)-C(7)-C(8)	122.3(9)	C(21)-C(28)-C(26)	119.4(9)
C(7)-C(8)-C(2)	121.2(8)	N(3)-C(29)-C(30)	177.2(9)
N(1)-C(9)-C(11)	113.0(7)	F(4A)-B(1A)-F(2A)	110.1(9)
N(1)-C(9)-C(10)	125.5(6)	F(4A)-B(1A)-F(1A)	112.4(8)
C(11)-C(9)-C(10)	121.5(7)	F(2A)-B(1A)-F(1A)	109.7(9)
N(2)-C(11)-C(9)	119.3(7)	F(4A)-B(1A)-F(3A)	109.2(9)
N(2)-C(11)-C(12)	119.9(6)	F(2A)-B(1A)-F(3A)	107.1(8)
C(9)-C(11)-C(12)	120.7(7)	F(1A)-B(1A)-F(3A)	108.1(8)
C(14)-C(13)-C(20)	119.6(7)		

Table S7. Anisotropic displacement parameters ($Å^2$ x 10^3) for **4b'**. The anisotropic displacement factor exponent takes the form: $-2\pi^2[h^2a^{*2}U_{11} + ... + 2hka^*b^*U_{12}]$

	U_{11}	U_{22}	U_{33}	U_{23}	U_{13}	U_{12}
Pt(1)	19(1)	17(1)	15(1)	-1(1)	0(1)	1(1)
N(1)	2(4)	20(4)	17(3)	-7(3)	4(3)	-3(3)
N(2)	15(5)	17(5)	8(3)	1(3)	1(3)	-11(4)
N(3)	18(5)	22(5)	28(4)	-6(4)	4(4)	-3(4)
C(1)	16(6)	17(5)	23(4)	6(4)	-7(4)	8(5)
C(2)	23(7)	7(6)	23(4)	-4(4)	8(4)	-1(5)
C(3)	23(6)	28(6)	23(4)	-7(5)	-4(4)	10(5)
C(4)	23(7)	35(7)	14(4)	2(4)	8(5)	-3(5)
C(5)	18(7)	35(7)	25(5)	-13(5)	1(5)	7(6)
C(6)	28(7)	46(7)	44(5)	1(5)	1(5)	-5(6)
C(7)	29(7)	37(7)	28(5)	2(5)	-6(5)	1(6)
C(8)	23(7)	35(7)	18(4)	2(4)	-7(5)	1(5)
C(10)	29(6)	20(6)	33(5)	3(4)	-12(4)	-3(5)
C(11)	8(5)	12(5)	9(4)	-1(4)	4(4)	-2(4)
C(12)	21(6)	12(6)	34(5)	1(4)	3(4)	8(5)
C(13)	20(7)	17(6)	21(4)	-15(4)	8(5)	-7(5)
C(14)	21(7)	19(6)	20(4)	1(4)	3(4)	-6(5)
C(15)	36(8)	11(6)	19(4)	-2(4)	0(4)	-7(5)
C(16)	33(8)	45(8)	26(5)	-1(5)	-9(5)	-9(5)
C(17)	42(8)	19(6)	15(4)	-4(4)	-4(5)	-7(5)
C(18)	38(7)	16(6)	19(4)	-2(4)	2(5)	-9(5)
C(19)	41(7)	49(7)	25(4)	4(5)	7(5)	-14(6)
C(20)	12(6)	20(6)	25(5)	1(4)	-3(4)	0(4)
C(21)	16(6)	21(6)	13(4)	7(4)	8(4)	6(5)
C(22)	22(6)	35(7)	18(4)	-4(5)	-3(4)	4(5)
C(23)	32(6)	21(6)	28(5)	8(5)	0(5)	4(6)
C(24)	44(7)	49(7)	34(5)	15(5)	14(5)	12(6)
C(25)	22(7)	44(8)	19(4)	13(5)	4(4)	12(5)
C(26)	23(6)	39(7)	20(4)	-15(5)	-15(4)	16(5)
C(27)	64(9)	56(8)	34(5)	-5(6)	-13(5)	8(7)
C(28)	27(6)	22(6)	21(4)	-3(5)	-3(4)	-4(5)
C(29)	19(6)	17(6)	15(4)	-1(4)	8(4)	1(5)
C(30)	22(6)	19(7)	48(6)	15(5)	10(5)	4(5)
B(1A)	29(9)	21(9)	54(7)	-9(7)	-4(8)	-13(8)
F(1A)	31(4)	27(3)	51(3)	10(3)	-4(3)	-4(3)
F(2A)	48(4)	92(5)	36(3)	-6(3)	-8(3)	-22(4)
F(3A)	35(3)	19(4)	73(4)	6(3)	14(3)	0(3)
F(4A)	43(4)	41(4)	53(3)	-1(3)	18(3)	28(3)

Table S8. Hydrogen coordinates (x 10^4) and isotropic displacement parameters (Å^2 x 10^3) for **4b'**.

	x	y	z	U(eq)
H(1A)	4828	5343	4313	22
H(1B)	3850	6047	4134	22
H(3)	4028	3925	4615	30
H(4)	2342	2820	4796	29
H(6A)	-903	2723	4604	59
H(6B)	-4	2479	4833	59
H(6C)	36	1505	4610	59
H(7)	-22	3909	4262	38
H(8)	1635	4998	4076	30
H(10A)	6564	1029	3392	41
H(10B)	7224	358	3620	41
H(10C)	7941	1509	3484	41
H(12A)	7401	402	4069	34
H(12B)	7970	1574	4222	34
H(12C)	8523	1276	3959	34
H(14)	3371	2798	3423	24
H(16A)	2163	3511	2834	51
H(16B)	1710	3426	3109	51
H(16C)	2095	2146	2966	51
H(17)	4402	3743	2744	30
H(19A)	6607	4704	2687	57
H(19B)	7318	3354	2724	57
H(19C)	7648	4538	2897	57
H(20)	7103	3490	3267	23
H(22)	5365	1222	4392	30
H(24A)	4433	1101	4943	63
H(24B)	5857	602	5000	63
H(24C)	5108	86	4767	63
H(25)	6397	2974	5010	34
H(27A)	8383	5179	4783	77
H(27B)	7439	5019	5009	77
H(27C)	7035	5919	4787	77
H(28)	7119	4682	4370	28
H(30A)	1659	5790	3325	44
H(30B)	2845	6723	3269	44
H(30C)	1840	7085	3477	44